OPEN ACCESS

Engineering of Conformal Electrode Coatings by Atomic Layer Deposition for Aqueous Na-ion Battery Electrodes

To cite this article: Laurynas Staišiūnas *et al* 2023 *J. Electrochem. Soc.* **170** 050533

Journal of The Electrochemical Society, 2023 **170** 050533

Engineering of Conformal Electrode Coatings by Atomic Layer Deposition for Aqueous Na-ion Battery Electrodes

Laurynas Staišiūnas,[1] Jurgis Pilipavičius,[1,2] Davit Tediashvili,[1,2] Jurga Juodkazytė,[1] and Linas Vilčiauskas[1,*,z]

[1]*Center for Physical Sciences and Technology (FTMC), Saulėtekio al. 3, LT-10257 Vilnius, Lithuania*
[2]*Institute of Chemistry, Vilnius University, Saulėtekio al. 3, LT-10257 Vilnius, Lithuania*

The application of atomic layer deposition on active material particles or as conformal layers directly on electrodes is an effective and viable approach for protecting the battery materials from degradation. Al_2O_3, TiO_2, and HfO_2 coatings are applied on $NaTi_2(PO_4)_3$, which is among the most studied negative electrode materials for aqueous Na-ion batteries. The coated electrodes are characterized in terms of electrochemical kinetics, charge capacity retention, and electrochemical impedance spectra. Al_2O_3, a widely used protective coating in non-aqueous batteries, is shown to be insufficient to suppress parasitic processes and is eventually dissolved by reaction with hydroxide during extended cycling in aqueous Na_2SO_4. However, this process provides a local buffering effect making the protective action of this coating mainly of chemical nature. TiO_2 is found to be very resistant to increase in pH and remains almost intact during electrochemical cycling. However, we provide strong evidence that TiO_2 itself is electrochemically active in aqueous electrolytes at negative potentials. The protonation of TiO_2 leads to an additional increase in local pH which is detrimental to $NaTi_2(PO_4)_3$ and results in even faster capacity loss than in uncoated electrodes. Only HfO_2 is found to be sufficiently stable and electrochemically inert ALD coating for negative $NaTi_2(PO_4)_3$ electrodes operating in aqueous electrolytes.

 [DOI: 10.1149/1945-7111/acd4ee]

Manuscript submitted February 22, 2023; revised manuscript received April 22, 2023. Published May 24, 2023.

Supplementary material for this article is available online

The increasing use of intermittent solar and wind energy requires new electrical energy storage solutions for balancing these sources in the electricity grids.[1,2] Electrochemical batteries stand as an attractive and promising technology due to their energy/power range, efficiency, and unique scalability. Lithium-ion battery technology is currently dominating the market in such sectors as consumer electronics and electric vehicles but also finds increasing use for large scale grid support. However, the expected massive deployment of grid-scale batteries raises growing concerns related to the supply of raw materials (lithium, cobalt, etc.), safety, and recycling issues. Therefore, there is an intensive search for alternative technologies with a considerable focus on the development of aqueous battery systems. Even though the narrow thermodynamic stability window of aqueous solutions limits the available energy density of such systems, it is the safety, high conductivity, environmental footprint, and low cost that make aqueous energy storage devices an attractive alternative for Li-ion batteries in the area of large-scale stationary storage. Aqueous sodium-ion batteries (ASIBs) have been attracting increasing attention, because of sodium abundancy, absence of cobalt, and the use of simple salt aqueous electrolytes. The variety of available electrode and electrolyte materials for ASIBs have been recently comprehensively reviewed.[3–5]

Among the sodium ion insertion materials, Na Super Ionic Conductors (NASICON) are of particular interest due to their high structural stability, ionic conductivity and variety of redox potentials, which depend on the selection of a transition metal.[6] NASICON-structured sodium titanium phosphate - $NaTi_2(PO_4)_3$ (NTP)—is one the most intensively studied negative electrode materials for ASIBs.[7,8] It has a relatively high theoretical capacity of 133 mAh g^{-1} and Na^+ ion intercalation potential of −0.6 V (SHE), which is very close to hydrogen evolution potentials in neutral media (−0.42 V (SHE)).[9] NTP was shown to have an outstanding rate capability,[10] which is due to extremely fast sodium ion insertion kinetics into its open 3D framework, as well as good cycling stability at fast charging rates.[8] However, it is also known that slow (⩽1C) galvanostatic charge/discharge cycling (GCD) of NTP anodes in aqueous electrolytes leads to low coulombic efficiency (CE) and fast capacity decay.[11–13] This has been attributed to the NTP degradation caused by increasing pH, which results from reduction of oxygen by $Ti^{(III)}$ in the charged form ($Na_3Ti_2(PO_4)_3$).[14] In addition to the dissolution of active material,[12] alkalization of electrolyte can also lead to the oxidation of the carbon additive, eventually resulting in the loss of electrical contact.[14] It has been suggested that the capacity fade of NTP electrodes can be caused by the formation of amorphous titanium phosphate or insoluble titanium sulfate phases which passivate the electrode surface.[13] In our recent study,[11] we did explicitly show that oxygen reduction related self-discharge of NTP plays a major role in the local pH increase, which causes the dissolution of active material and the formation of amorphous Ti-rich insoluble interfacial layer similar to the solid electrolyte interphase (SEI) in non-aqueous batteries. However, these in situ formed interphasial layers are relatively unstable and do not provide sufficient protection from further material degradation. Therefore, other more effective protection methods are in high demand in the field of aqueous battery systems.

There are several ways to mitigate the detrimental interactions at the aqueous electrode-electrolyte interface. One is based on the use of hybrid (water + organic solvent) or highly concentrated (water-in-salt) electrolytes. Such electrolytes display reduced water activity and oxygen solubility or even might be electrochemically unstable and form a passivating layer from the decomposition products.[15] This was shown to stabilize NTP capacity fade to some extent.[16,17] Another strategy is to deliberately apply protective coatings to prevent direct contact between the active electrode material and electrolyte solution. Such coating should be sufficiently thin to ensure low impedance (i.e. good ionic and electronic conductivity), and be conformal (i.e. form a continuous layer). For example, there have been attempts to utilize conductive carbon protective particle shells.[18,19] An alternative approach is based on the use of Atomic Layer Deposition (ALD) technique. ALD is regarded as a powerful interface engineering tool due to its atomic scale precision in controlling layer thickness, supreme uniformity and conformity, which makes the coating of high aspect ratio structures at low deposition temperatures possible. Moreover, this technique has

*Electrochemical Society Member.
[z]E-mail: linas.vilciauskas@ftmc.lt

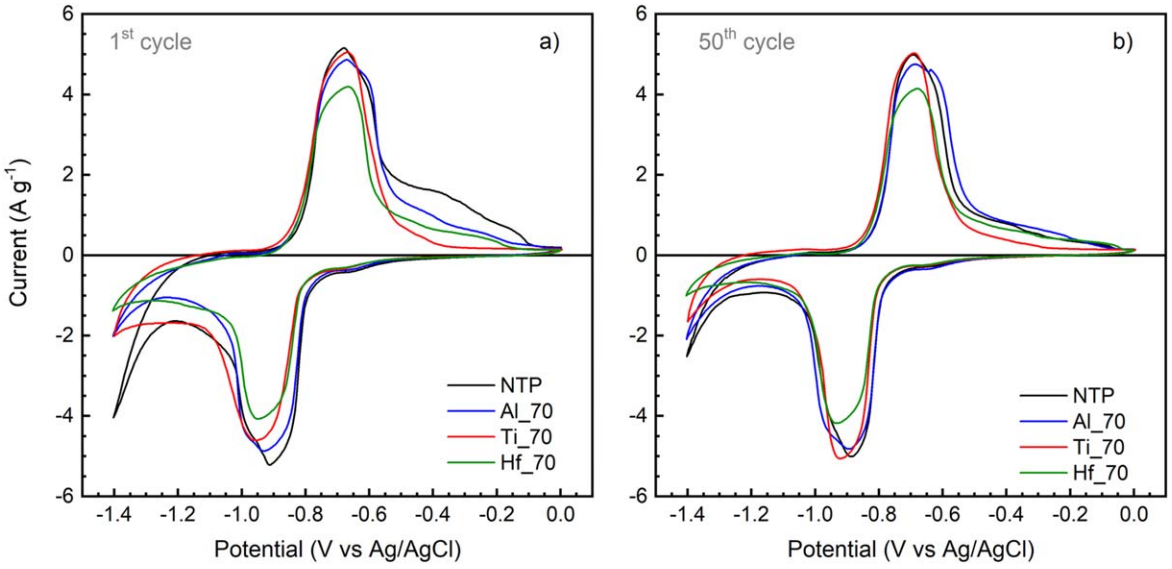

Figure 1. Cyclic voltammograms of uncoated and ALD-coated Al_70, Ti_70 and Hf_70 electrodes (a) 1st and (b) 50th CV cycles recorded in 1 M Na_2SO_4 (aq.) at 5 mV s^{-1}.

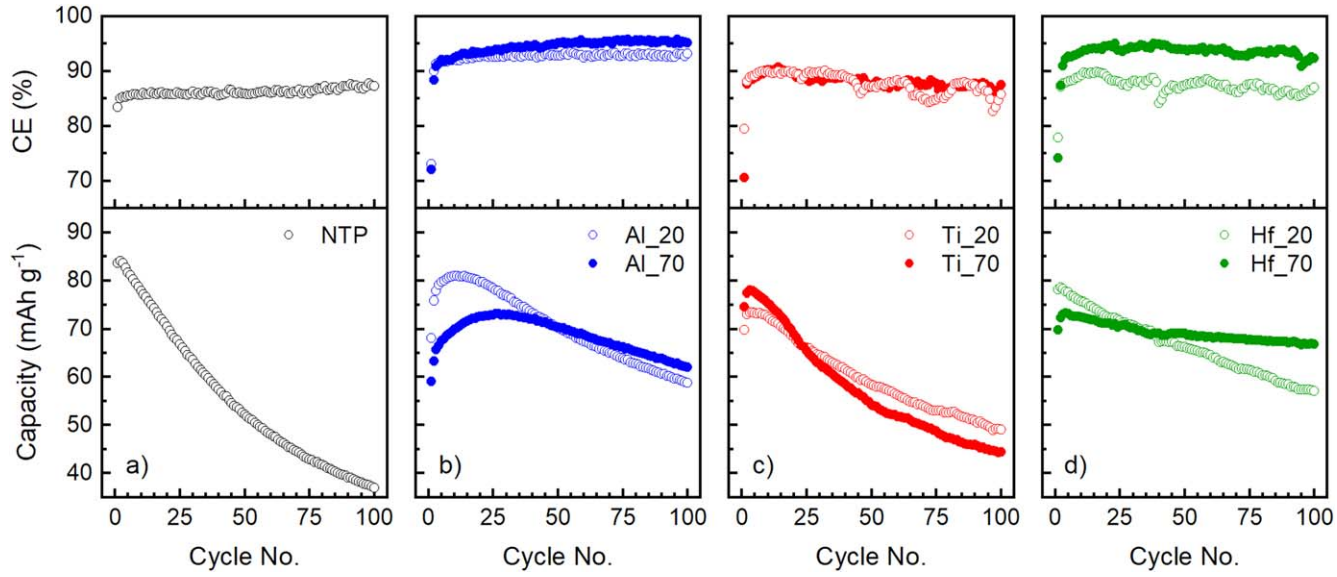

Figure 2. Variation of specific discharge capacity and Coulombic efficiency of (a) uncoated NTP, (b) Al_2O_3−, (c) TiO_2−, and (d) HfO_2-coated NTP electrodes during GCD cycling at 1C (0.133 A g^{-1}) rate in 1 M Na_2SO_4 (aq.) electrolyte.

already found industrial large-scale applications.[20] Recent progress of ALD coatings in battery applications, including sodium ion batteries (SIBs), was previously summarized.[21–25] Nanometric Al_2O_3, TiO_2 and HfO_2 coatings have already been tested for organic SIB anodes.[24] Significant improvements in cycling stability and capacity retention of various SIB electrode materials in organic electrolytes have been reported, whereas the protective ability of ALD coatings in the case of aqueous media has received significantly less attention.[11,26]

There are two possibilities for applying ultrathin ALD coatings in the formation of protective barrier layers on active electrode materials: (1) coating of the active material powder resulting in core–shell particle structures[5] or (2) depositing the coating directly on the electrode surface.[27,28] The first approach requires special equipment such as a fluidized particle bed or drum reactors. The process could be complicated due to particle agglomeration and core–shell configuration which might have adverse effects on material conductivity.[5,29] On the other hand, the formation of ALD layers directly on top of the electrode surface is technically simpler, making processing of large areas and batches feasible. The coating of only the electrode surface does not compromise the conductivity but can suppress parasitic reactions such as oxygen reduction, hydrogen evolution, carbon oxidation, oxygen evolution, etc.[26]

In the present study, Al_2O_3, TiO_2, and HfO_2 coatings of varying thickness were applied on the surface of $NaTi_2(PO_4)_3$ electrodes using ALD. The effects of these coatings on preventing the parasitic reactions leading to self-discharge and capacity fade of the electrodes in aqueous electrolytes were carefully analyzed using electrochemical techniques such as galvanostatic charge/discharge cycling, and electrochemical impedance spectroscopy as well as X-ray photoelectron scpectroscopy (XPS) and energy dispersive X-ray spectroscopy (EDX). The results show that, although widely employed, Al_2O_3 and TiO_2 coatings are not electrochemically stable or inactive during extended charge/discharge cycling and do not provide sufficient protection of $NaTi_2(PO_4)_3$ especially in alkaline or

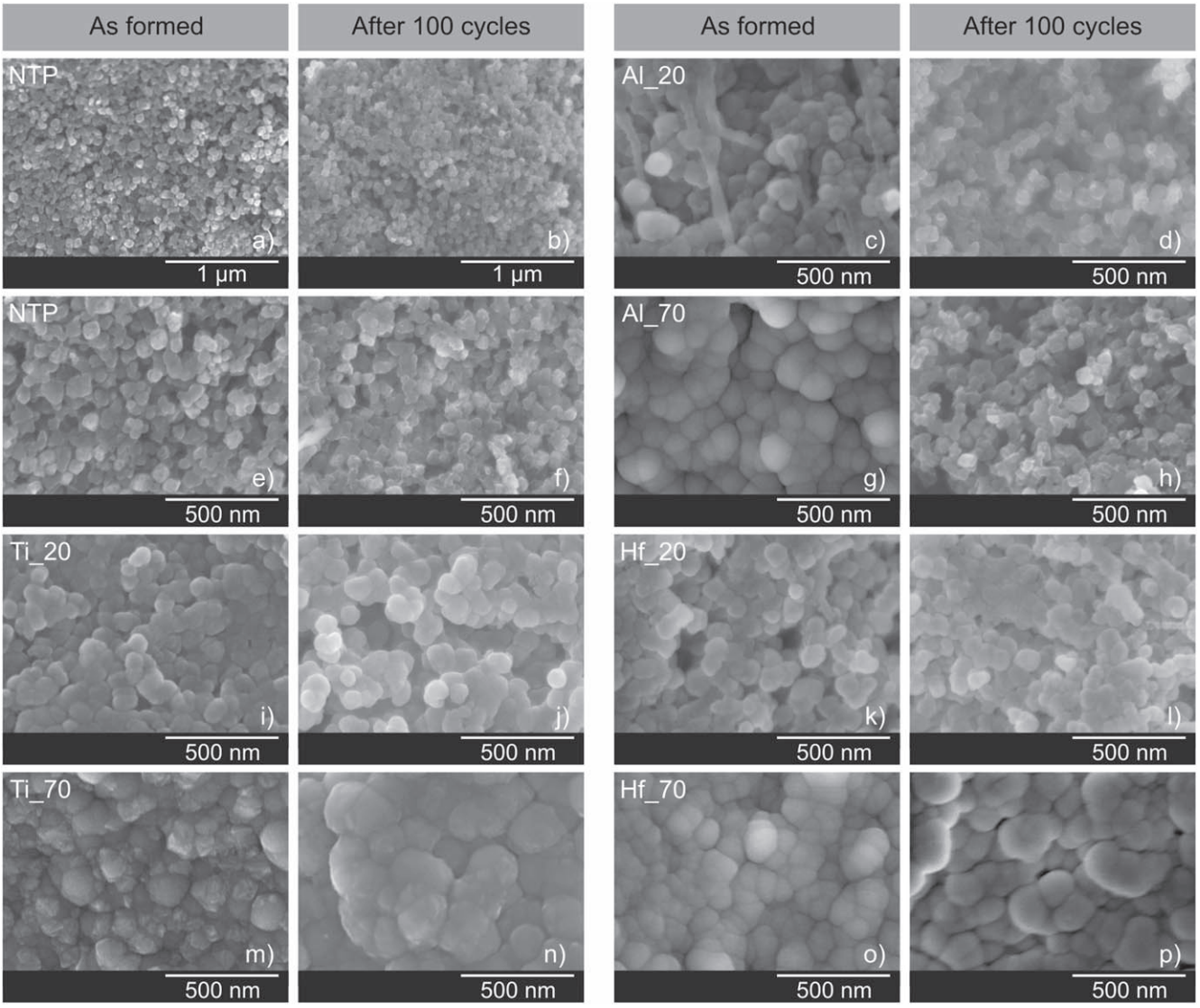

Figure 3. Top view SEM images of uncoated NTP (a), (b), (e), (f) and Al_2O_3−, TiO_2−, HfO_2-coated NTP electrodes: Al_20 (c), (d), Al_70 (g), (h), Ti_20 (i), (j), Ti_70 (m), (n), Hf_20 (k), (l) and Hf_70 (o), (p) electrodes before (a), (e), (i), (m), (c), (g), (k), (o) and after 100 GCD cycles in 1 M Na_2SO_4 (aq.) at 1C rate.

near alkaline conditions. On the other hand, HfO_2 is shown to be very stable under the typical ASIB operating conditions, effectively suppressing parasitic reactions, protecting the electrode from degradation and preventing capacity loss.

Experimental

Material synthesis and electrode preparation.—Nanosized $NaTi_2(PO_4)_3$ used in this work was synthesized via solvothermal method using a previously described methodology.[11,30] CH_3COONa (Chempur, ⩾99.0%) was first dissolved in H_3PO_4 (Reachem, 85 wt%), then CH_3COOH (Lach-ner, 99.8%) together with CH_3CH_2OH (Honeywell, ⩾99.8%) were subsequently added to the mixture. Then, a solution of $C_{16}H_{36}O_4Ti$ (1.4 ml, Acros Organics, ⩾98%) in CH_3CH_2OH (10 ml) was prepared and added dropwise into the initial mixture under vigorous magnetic stirring. After continuous stirring for 30 min at room temperature, the obtained transparent final solution was transferred into a 100 ml Teflon-lined stainless-steel autoclave which was heated to 120 °C–200 °C and kept for 12 h. Eventually, the obtained white precipitate was collected by centrifugation and washed several times with distilled water and ethanol subsequently followed by drying at 80 °C overnight. The resulting NTP powder was coated with a layer of carbon by first homogeneously mixing 0.6 g of additionally ball-milled (1 h at 900 rpm) powder and glucose (0.15 g) in distilled water (50 ml) and then heating the resulting mixture at 60 °C under magnetic stirring. The obtained slurry was subsequently dried at 80 °C for complete water elimination and the obtained powder was reground and annealed at 700 °C for 2 h in N_2 atmosphere in order to pyrolyze the glucose. The carbon loading on active material particles as determined by thermogravimetry is approximately 4 wt%.

The electrode slurry was prepared by mixing 70 wt% of active material, 20 wt% of carbon black (CB) (Super-P, TIMCAL) and 10 wt% of polyvinylidene fluoride (PVDF) (HSV1800, Kynar) in N-methyl-2-pyrrolidone (NMP) (Sigma Aldrich, 99.5%). The slurry was homogenized in a planetary ball-mill (Retsch PM 400) for 1 h at 900 rpm, then casted as a film and dried in vacuum for 3 h at 120 °C. Obtained films were transferred on 316 L grade stainless steel mesh disks of approx. 1.3 cm^2 by pressing. The average active material load was 2.0 ± 0.3 mg per electrode.

Atomic layer deposition.—The electrodes were coated by Al_2O_3, TiO_2 and HfO_2 using ALD in the exposure mode, which is based on a prolonged substrate exposure to precursors allowing the coating of highly structured surfaces. All coatings were deposited at 170 °C reactor temperature in Fiji F200 ALD deposition system

Table I. The nomenclature of samples used in this work.

Sample	Coating material	Number of ALD cycles	Coating thickness
NTP	—	—	0 nm
Al_20	Al_2O_3	150	19 nm
Al_70	Al_2O_3	600	75 nm
Ti_20	TiO_2	400	20 nm
Ti_70	TiO_2	1400	71 nm
Hf_20	HfO_2	150	18 nm
Hf_70	HfO_2	600	73 nm

(CambridgeNanotech). Trimethylaluminum ($Al_2(CH_3)_6$), tetrakis(dimethylamino) titanium ($Ti(N(CH_3)_2)_4$) and tetrakis(dimethylamino) hafnium ($Hf(N(CH_3)_2)_4$) (all >98% purity, obtained from Strem) were used as Al, Ti and Hf precursors, respectively. Deionised H_2O was used as an oxygen source. A constant flow of 140 sccm of Ar as a carrier gas was used during the deposition processes, resulting in 0.3 mbar of base pressure in the reaction chamber. The deposition cycle consisted of a sequence of 0.2 s precursor pulse, 20 s exposure time, 20 s purge time, 0.2 s deionized water pulse, 20 s exposure time and 20 s purge time. During the layer deposition process, a small piece of Si wafer was simultaneously coated in the same chamber and later used for the determination of coating thickness. The ALD layer thickness on the Si wafer was measured using a dual rotating compensator ellipsometer (RC2, J.A. Woollam, Co., Inc.) in the 300 nm–900 nm spectral range. This result was used as a proxy quantity for estimating the layer thickness on highly structured 3D electrode surfaces.

Electrochemical characterization and analysis.— Electrochemical analysis was performed in a three-electrode cell with graphite rod electrode as counter and Ag/AgCl (3.5 M KCl) as reference electrode, respectively. All potentials in this work are referenced with respect to Ag/AgCl electrode unless noted otherwise. 50 ml of naturally aerated 1 M Na_2SO_4 (aq.) solution in deionized water was used as electrolyte. Cyclic voltammetry (CV) and galvanostatic charge/discharge (GCD) measurements were performed on PGSTAT302 (Methrom-Autolab) electrochemical workstation. All specific current values are normalized to the active material weight in the electrode.

CV measurements were performed in the potential range from 0 to −1.4 V vs Ag/AgCl at 5 mV s^{-1} potential scan rate. A total of 50 CV cycles were recorded for every sample.

GCD experiments were performed in a potential range from −0.6 V to −0.9 V vs Ag/AgCl. The electrodes were cycled at 1C (0.133 A g^{-1}) rate corresponding to the theoretical capacity of NTP (0.133 Ah g^{-1}). A 10 s rest period was set after a complete charge and discharge cycle.

The electrochemical activity of TiO_2 coatings was separately checked by an additional experiment. For this, a 6 mm diameter and 40 mm length clean graphite rod (Alfa Aesar) was coated with 70 nm TiO_2 using an identical ALD protocol as in all experiments. CVs were recorded for an uncoated reference and TiO_2 coated graphite rods in the range from 1.0 to −1.4 V vs Ag/AgCl.

Electrochemical impedance spectroscopy (EIS) investigations were carried out using Zahner Zennium (ZAHNER-elektrik GmbH & Co. KG.) potentiostat/galvanostat and frequency analyzer. Electrodes for EIS analysis were smaller with an area of 0.13 cm^2 in order to increase the impedance to measurable levels, as very low impedance of the electrode and relatively high interfacial contact resistance results in very noisy data. Measurements were performed at the approximate midpoint of discharge (plateau region) on the 1st, 2nd, 5th, 10th, 50th and 100th cycles. The estimation of an approximate midpoint was made from the discharge time of a previous cycle i.e. assuming that capacity fade in a single GCD cycle is relatively small. EIS was performed in potentiostatic mode, allowing 10 s of setting time after charging current was turned off, in the range of 0.1 Hz to 10 kHz and 5 mV excitation amplitude. EIS spectra were fitted using an in-house modified version of *impedance.py* package.[31] The uncompensated resistance comprising electrolyte and contact resistances and approximately equal to 5 Ω for uncoated and 7–10 Ω for ALD-coated electrodes was removed from the displayed results after fitting, for better representation of data.

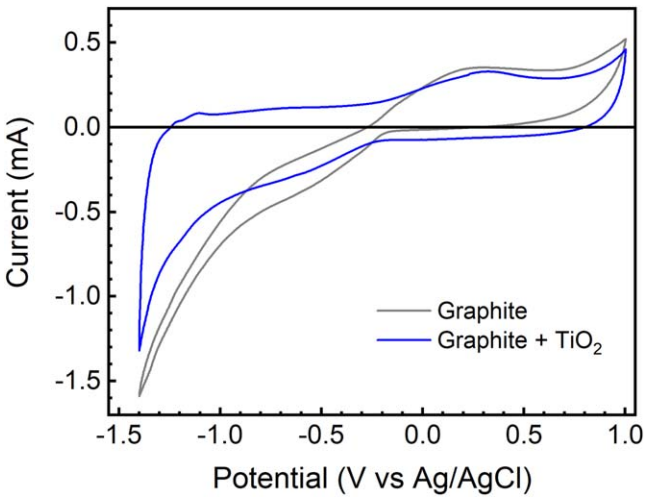

Figure 4. Cyclic voltammograms of clean graphite rod and graphite rod with ALD-coated 70 nm amorphous TiO_2 layer recorded in 1 M Na_2SO_4 (aq.) at 5 mV s^{-1}.

Scanning electron microscopy (SEM) and energy dispersive X-ray spectroscopy (EDX).— High-resolution SEM micrographs of NTP electrodes were recorded on Hitachi SU-70 microscope using 5.0 kV acceleration voltage at the center of an electrode. Electrode cross-section SEM/EDX maps were acquired on a Hitachi TM-6000 microscope using 15 kV acceleration voltage. For this purpose, the electrodes at the center were cut in half and placed perpendicular to the electron beam. For all samples, the EDX map collection time was fixed to 3 min.

X-ray photoelectron spectroscopy (XPS).— XPS analyses were performed on Kratos Axis Supra spectrometer using monochromatic Al-K_α radiation ($h\nu = 1486.7$ eV) with X-ray gun power of 225 W at 10^{-8} torr pressure and room temperature. The analyzed area at the sample center was approximately 0.16 mm^2 in size and high-resolution selected area scans were acquired using pass energy of 20 eV. In order to compensate for sample charging during the measurement, a built-in charge neutralizer was used. The samples were also electrically isolated from the sample holder bar in order to avoid preferential charging effects. Binding energy scale of recorded spectra was corrected by referencing to C 1s peak at 284.8 eV. The peak fitting of recorded spectra was performed using Kratos Escape software. Shirley background function was applied for fitting the Ti $2p_{3/2}$ and C 1s spectra whereas a linear background function was used for Ti $2p_{1/2}$.

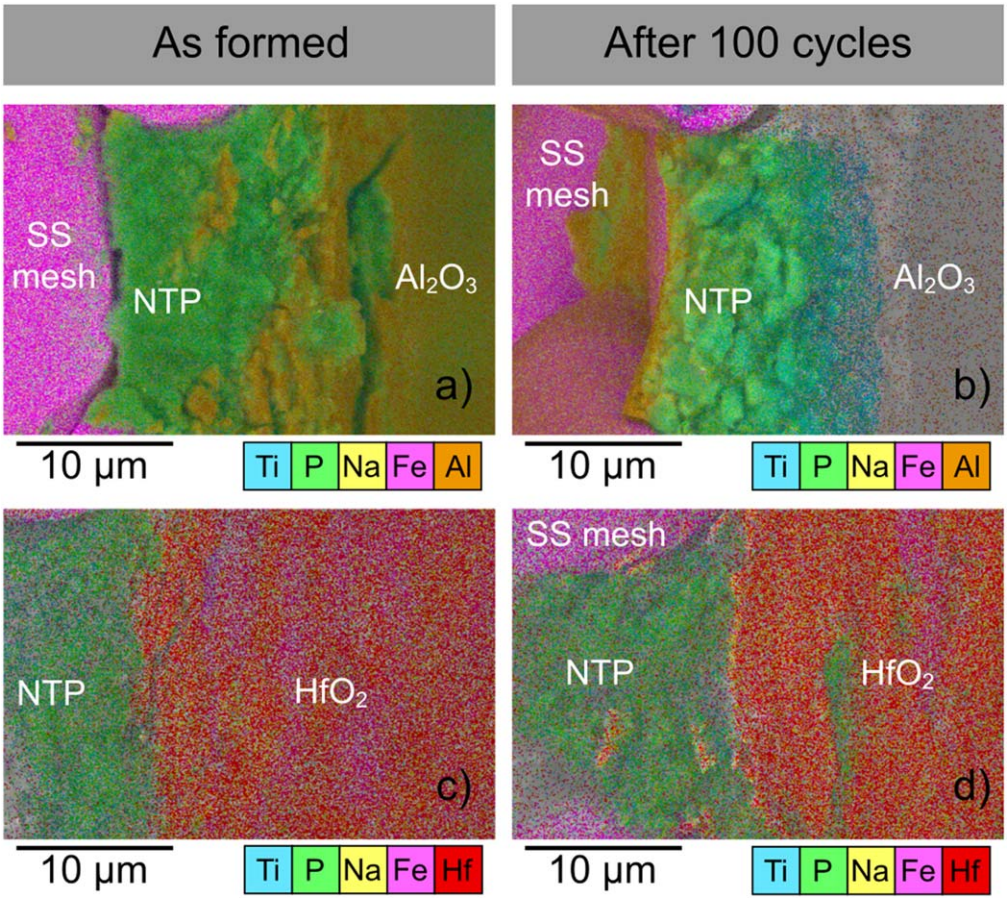

Figure 5. Tilted cross-sectional view with EDX elemental mapping of fresh and cycled ALD-coated electrodes: (a, b) Al_70 and (c, d) Hf_70 before (a, c) and after 100 GCD cycles, respectively, in 1 M Na_2SO_4 (aq.) at 1C rate.

Results and Discussion

Cyclic voltammetry and galvanostatic charge/discharge cycling.—NTP electrodes were coated by Al_2O_3, TiO_2 and HfO_2 using a varying number of ALD cycles in order to achieve two coating thicknesses of approx. 20 nm and 70 nm for each oxide, respectively. The different coating thickness was selected for comparative purposes with a belief that such layers would yield qualitatively different properties in terms of ionic transport and protective ability. In addition, the previous experience dictates that HfO_2 starts to change from amorphous to crystalline at ca. 80 nm. The approximate growth rate was 0.13 nm/cycle for Al_2O_3, 0.12 nm/cycle for HfO_2 and 0.05 nm/cycle for TiO_2. The resulting thickness as measured by spectroscopic ellipsometry on a simultaneously coated Si wafer is presented in Table I. The sample nomenclature as presented in Table I will be used throughout this work.

At first, the electrodes were characterized by means of cyclic voltammetry in 1 M Na_2SO_4 (aq.) electrolyte. Obtained CVs of uncoated NTP and Al_70, Ti_70 and Hf_70 electrodes are presented in Fig. 1. A pair of cathodic and anodic current peaks representing $Ti^{(IV)}/Ti^{(III)}$ redox process accompanied by insertion/extraction of Na^+ ions is visible in all samples. The deposition of 70 nm thick oxide layers has negligible influence on the NTP electrochemical redox kinetics. Only in the case of Hf_70 the decrease in peak currents was more noticeable suggesting that hafnia layer might be more compact and has a slightly stronger blocking nature than other oxides (Fig. 1). One of the differences between the uncoated and coated NTP electrodes can be seen in the potential ranges outside the main redox processes, i.e. at $E < -1.2$ V and $E > 0.6$ V, respectively (Fig. 1a). The observed increase in current at $E < -1.2$ V is attributed to the onset of hydrogen evolution reaction (HER). The highest current, i.e. the lowest HER overpotential is observed in the case of an uncoated NTP sample, whereas on a HfO_2-coated electrode the kinetics of this parasitic process is slower (Fig. 1a). The effective suppression of HER by ALD-formed Al_2O_3 on $Li_4Ti_5O_{12}$ has been reported, previously.[32] A slight shift in the cathodic peaks can be attributed to some additional polarization resistance on these samples, or it could be related to the cathodic stability of TiO_2 and HfO_2 vs Al_2O_3. After 50 CV cycles in the 0 V to −1.4 V range, the voltammetric peaks become slightly narrower (Fig. 1b), which could be explained either by the degradation of electrode material via partial dissolution or/and passivation of the electrode surface by degradation products. The electrochemical kinetics of HER on an uncoated NTP electrode after 50 CV cycles becomes slower, which can also be a result of HER potential shift to lower values due to increase in local pH or aforementioned surface passivation. The CVs of a Hf_70 sample after 50 cycles still exhibit slightly lower current peaks as well as the lowest current in the HER region ($E < -1.2$ V) among the studied samples (Fig. 1b).

The results of GCD cycling are summarized in Fig. 2. The capacity retention of electrodes was evaluated as the ratio of the lowest and the highest discharge capacity values. One can see that in a given set, the capacity fade of uncoated NTP electrodes during GCD cycling was significant with only 44% of the initial capacity left after 100 cycles (Fig. 2a). Moreover, the Coulombic efficiency (CE) was also relatively low, staying below 90% throughout the experiment. This points to the significant influence of parasitic reactions, the most probable of which are oxygen reduction (ORR) and hydrogen evolution reactions.[11] The deposition of nanometric layers of alumina on the surface of NTP electrodes leads to a marked improvement in both the capacity retention, 72% and 84% for Al_20 and Al_70, respectively, and CE 92%–95% (Fig. 2b). It is noteworthy that initial capacities of these samples and especially

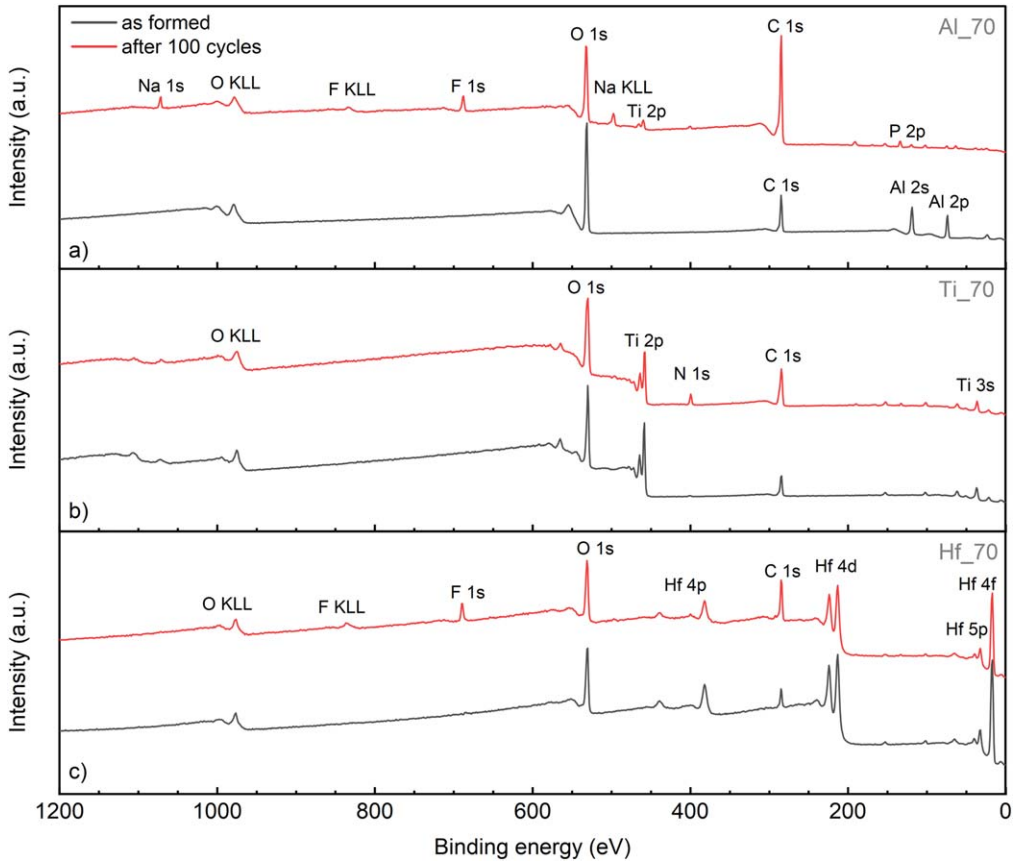

Figure 6. XPS survey spectra of ALD-coated NTP electrodes before (black line) and after (red line) 100 GCD cycles in 1 M Na_2SO_4 (aq.) at 1C rate: (a) Al_70, (b) Ti_70 and (c) Hf_70.

in the case of thicker Al_70 coatings are slightly lower compared to those of uncoated NTP. Interestingly, they are also slightly increasing during the first 10–20 cycles and only then start to decrease. The capacity retention of TiO_2-coated samples was slightly better than of uncoated NTP, but lower than Al_2O_3-coated NTP (Fig. 2c). Interestingly, a thinner TiO_2 coating was even slightly more efficient in terms of capacity retention, i.e. 67% vs 57% for Ti_20 and Ti_70 samples, respectively. Similarly to Al_2O_3-coated samples, a slight and steady increase in discharge capacity was observed during the first 5 cycles, whereas CE values were close to those of uncoated NTP and practically independent on the thickness of TiO_2 coating (Fig. 2c). However, in the case of HfO_2 coated NTP, significantly stronger effects of the protective layer are observed (Fig. 2d). NTP electrode coated with a 70 nm layer of HfO_2 outperformed all the other samples in terms of capacity retention (91%) and considerably higher CE value of ∼94% (Fig. 2d). In general, the initial capacities of ALD-coated electrodes are only 4% to 12% lower compared to those of uncoated samples, further suggesting that the ion insulating/blocking effect of thin oxide coatings is not significant. In order to gain a deeper insight into the origins of different performance of ALD-coated NTP electrodes, a set of detailed SEM, EDX and XPS investigations of the samples before and after GCD cycling were performed.

SEM, EDX and XPS characterization.—SEM images displaying the morphology of coated and uncoated NTP electrodes before and after GCD cycling are presented in Fig. 3. In Figs. 3a and 3e one can see that solvothermally synthesized NTP is composed of cube-shaped nanoparticles with dimensions ranging between 50 and 100 nm. The electrodes after 100 GCD cycles in 1 M Na_2SO_4 (aq.) (Figs. 3b and 3f) look very similar to as-prepared samples (Figs. 3a and 3e). Only, the particles seem to be a little smaller and have surface defects, very similar to those reported in Ref. 12 after treatment of NTP in alkaline medium (pH > 13). The deposition of a 20 nm thick layer of Al_2O_3 led to a noticeable increase in particle size (Fig. 3c) and a coalescence of globules at larger coating thickness (Fig. 3g). However, after 100 GCD cycles the morphology of the electrode strongly resembles that of uncoated NTP (Fig. 3e). This suggests that the majority of alumina coating is dissolved during cycling. Al_2O_3 is unstable in alkaline conditions and most likely dissolves due to an increase in local pH caused by parasitic processes. The presence of dissolved Al in 1 M Na_2SO_4 (aq.) electrolyte after cycling of ALD alumina-coated NTP was previously reported as well.[11] The electrode unblocking due to partial alumina dissolution might be one of the main reasons for the observed increase in discharge capacities in the first 10 to 20 GCD cycles (Fig. 5b). Although the capacity retention and CE of Al_2O_3-coated NTP electrodes are better than those of the uncoated electrodes, such coatings are obviously not sufficiently stable under studied conditions. Moreover, the observed protective capability is most likely of chemical nature due to the local buffering coming from the reaction of Al_2O_3 with hydroxide.

The morphology of NTP electrode with 20 nm coating of TiO_2 (Fig. 3i) looks very similar to that of the Al_2O_3-coated Al_20 sample (Fig. 3c), whereas the Ti_70 electrode looks different (Fig. 3m). The surface of globules is not as smooth and the presence of crystallites with sharper edges can be observed. Interestingly, after 100 GDC cycles, almost no change in particle morphology could be observed for TiO_2-coated NTP electrodes (Figs. 3j and 3n), except that the surface of Ti_70 looked smoother with slightly enlarged particles. This was an unexpected result, considering that capacity retention and CE of Ti_20 and Ti_70 samples are lower than those of Al_2O_3-coated NTP electrodes (Fig. 2). These results are also in contrast to the previously reported protective ability of amorphous

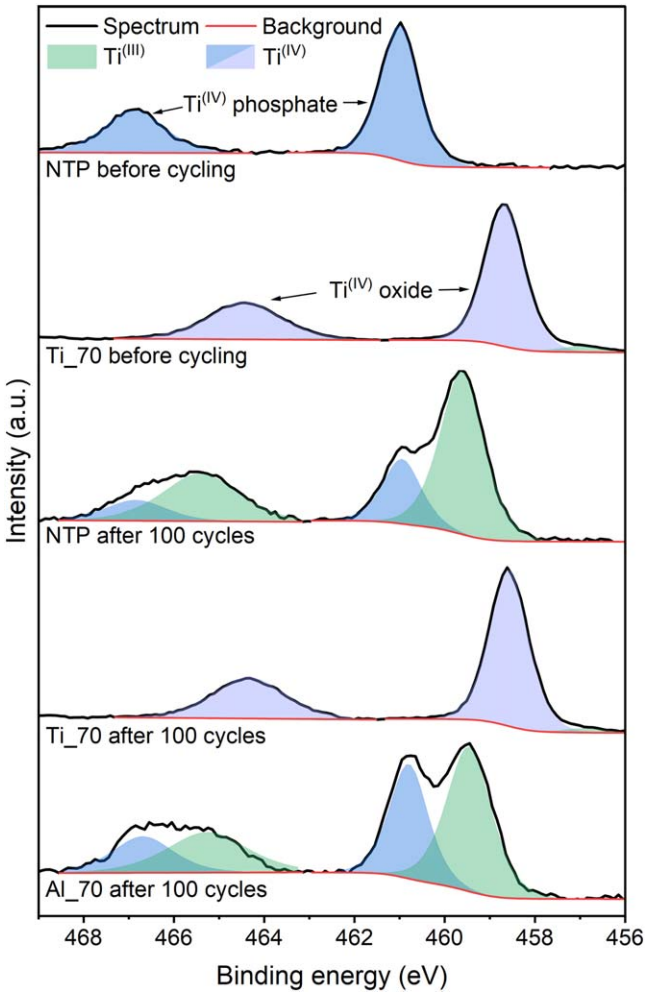

Figure 7. Comparison of high-resolution Ti 2p XPS spectra of: (top to bottom) as-prepared uncoated NTP; as-prepared Ti_70; uncoated NTP after 100 GCD cycles; Ti_70 after 100 GCD cycles; Al_70 after 100 GCD cycles.

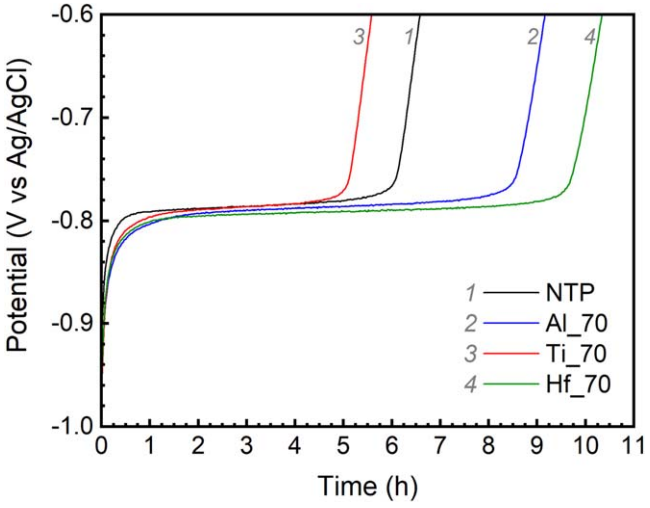

Figure 8. Self-discharge kinetics of uncoated NTP, Al_70, Ti_70 and Hf_70 electrodes after charging them at 1C rate in 1 M Na_2SO_4 (aq.) under ambient conditions.

TiO_2 sol-gel coating on analogous $LiTi_2(PO_4)_3$.[33] The CE of about 90% implies that TiO_2 does not suppress the parasitic ORR and/or HER taking place during charging and discharging, but the coating itself is sufficiently resistant to local changes in pH induced by these reactions. It is also very likely that TiO_2 is electrochemically active within the studied potential range, undergoing reversible redox transition between $Ti^{(III)}$ and $Ti^{(IV)}$ states according to the reaction:

$$Ti^{(IV)}O_2 + xH_2O + xe^- \leftrightarrows Ti^{(IV)}_{1-x}Ti^{(III)}_xO_{2-x}(OH)_x + xOH^- \quad [1]$$

According to Ref. 9, for Reaction 1, $E^0(TiO_2/Ti_{1-x}Ti_xO_{2-x}(OH)_x) = (-0.091–0.0591\ pH)$ V or $E^0(TiO_2/Ti_2O_3) = (-0.556–0.0591\ pH)$ V if anhydrous oxide phases are considered. Such electrochemical proton insertion into amorphous TiO_2 has been recently reported.[34–36] The mechanism leading to an additional increase in local pH could explain why the capacity fade of Ti_70 with thicker ALD coating was even faster than that Ti_20. In order to verify this hypothesis, an additional experiment was carried out in order to test the electrochemical response of TiO_2 itself. For this purpose, an amorphous 70 nm thick layer of titania was deposited on a clean graphite rod surface using exactly the same ALD protocol as in the case of Ti_70 electrode. The CV results for a reference graphite rod and one covered by TiO_2 layer are displayed in Fig. 4. The initial cleaning CV cycle is omitted from data presentation and the subsequent voltammograms do not significantly change anymore. The results in Fig. 4 show a clear reversible electrochemical response of TiO_2 in the studied potential range supporting our view that Reaction 1 might be taking place on the electrode together with the main redox processes of NTP.

The surface morphology of freshly HfO_2-coated electrodes (Figs. 3k and 3o) looks very similar to Al_2O_3-coated ones (Figs. 3c and 3g). However, in contrast to other types of coatings the morphology of Hf_20 and Hf_70 samples after 100 GCD cycles in 1 M Na_2SO_4 (aq.) remains practically unchanged (Figs. 3l and 3p). In terms of capacity retention and CE, a 20 nm thick layer of HfO_2 is obviously still insufficient to suppress the influence of parasitic processes, whereas the Hf_70 sample outperformed all of the electrodes studied in this work (Fig. 2). This suggests that among studied oxides, HfO_2 is the only coating which is sufficiently stable in aqueous NTP operating conditions. In order to achieve a perfect balance between the blocking and protective effects it still needs to be carefully optimized in terms of thickness and conformity by adjusting the ALD parameters for the best coating properties.

The elemental distribution on the surface of fresh and cycled electrodes was analyzed with the help of EDX spectroscopy and the results are presented in Fig. 5. The TiO_2-coated electrodes were omitted from this analysis because it is not possible to distinguish the Ti present in the NTP substrate from that in the ALD coating. The EDX elemental maps of Al_70 and Hf_70 samples before and after 100 GCD cycles confirm the previous results that most of the alumina ALD coating is dissolved during cycling (Figs. 5a and 5b), whereas hafnia remains practically intact (Hf is represented by red color in Figs. 5c and 5d). Only some small cracks can be seen in HfO_2 layer after GCD cycling, which might be a result of mechanical stress or slight swelling of the underlying electrode.

More detailed analysis of the chemical composition of uncoated NTP and ALD-coated electrode surface before and after GCD cycling was performed by means of X-ray photoelectron spectroscopy . XPS survey spectra of Al_70, Ti_70 and Hf_70 electrode samples are presented in Fig. 6. The spectrum of freshly formed alumina coating displays Al 2p peak at 74.1 eV attributable to Al in Al_2O_3, whereas the Ti 2p, P 2p, and F 1 s peaks respectively at 459.6 eV, 134 eV and 688 eV and corresponding to NTP and PVDF binder, are absent (Fig. 6a). This demonstrates that a 70 nm thick ALD coating coats the electrode surface continuously. However, significant changes are observed after 100 GCD cycles: the Al 2p peak is practically absent, while the Ti 2p, P 2p, and F 1 s signals become visible and the intensity of C 1 s peak increases notably. In fact, the Al 2p signal is practically invisible after 15 cycles. These results are consistent with the SEM and EDX data (Figs. 3d and 3h, and 5a and 5b) and confirm our hypothesis of the initial capacity increase of alumina coated NTP electrodes being related to the

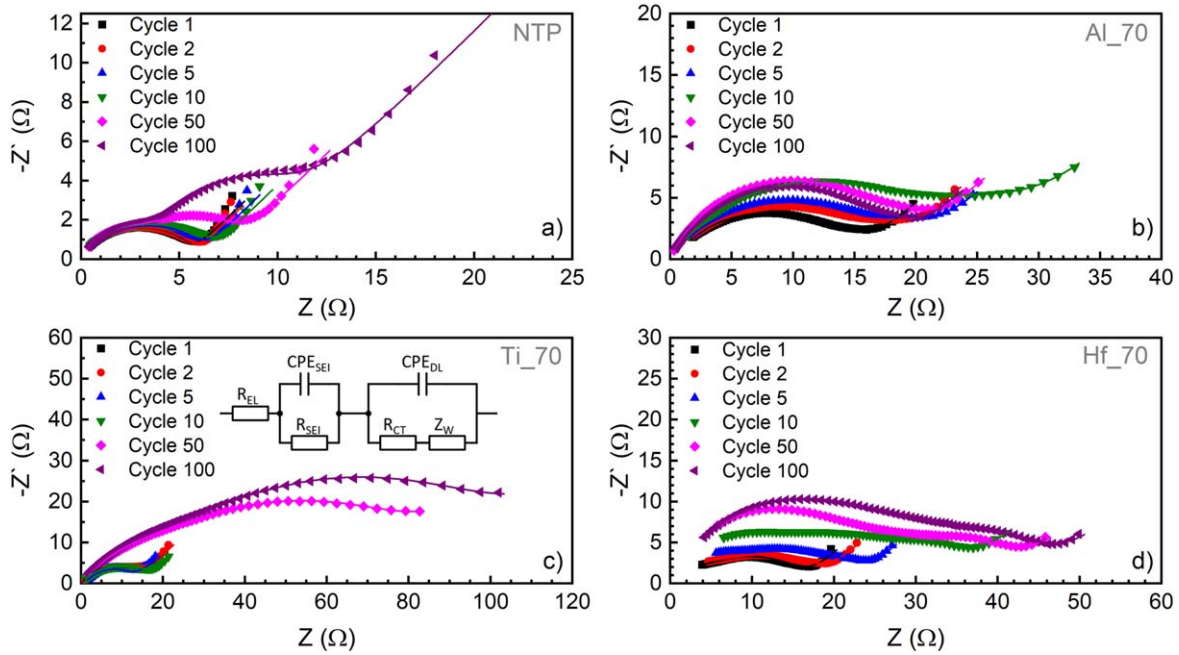

Figure 9. Impedance spectra of (a) uncoated NTP, (b) Al_70, (c) Ti_70, and (d) Hf_70 electrodes. Measurements were performed at the approximate midpoint of discharge plateau on the 1st, 2nd, 5th, 10th, 50th and 100th cycles performed at 1C rate in 1 M Na_2SO_4 (aq.) (symbols - experimental data, lines - fitted data). Inset in (c) shows the equivalent circuit used to fit the impedance data.

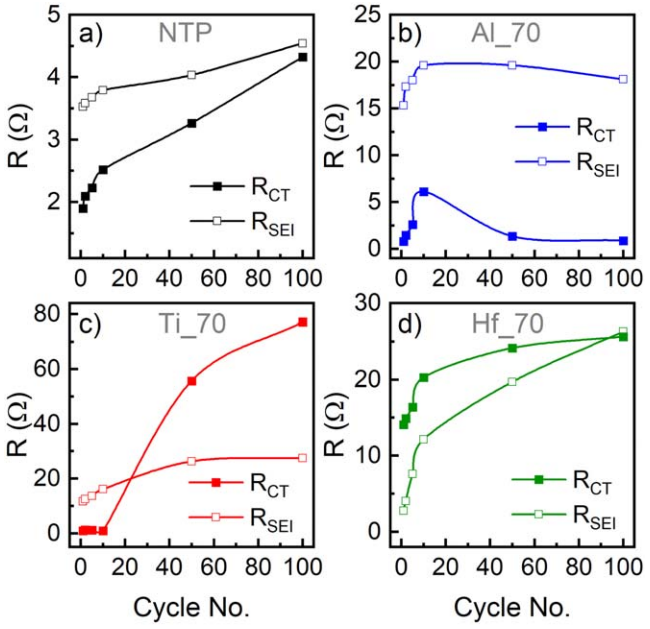

Figure 10. EIS fitted R_{CT} and R_{SEI} values for NTP electrodes during GCD cycling. (a) uncoated NTP, (b) Al_70, (c) Ti_70, and (d) Hf_70 cycled at 1C rate in 1 M Na_2SO_4 (aq.).

dissolution of Al_2O_3, whereas further capacity decay being related to the degradation of exposed NTP (Fig. 3b). This is further supported by the analysis of high resolution Ti 2p spectra shown in Fig. 7. The peak at 461 eV in the Ti 2p spectrum of as-prepared NTP electrode is attributed to Ti $2p_{2/3}$ line of $Ti^{(IV)}$ state in $NaTi_2(PO_4)_3$.[13,37] After 100 GCD cycles the intensity of this peak decreased significantly and another more intensive feature at lower binding energy values (459.6 eV) appears. The latter feature is traditionally attributed to the $Ti^{(III)}$ present in the NTP or its degradation products.[11,13] A very similar pair of peaks corresponding to the same binding energy is also observed in the XPS spectrum of Al_70 electrode after 100 GCD cycles (Fig. 7). XPS survey spectra of fresh and cycled Ti_70 electrodes are almost identical (Fig. 6b). However, the high-resolution Ti 2p spectra reveal a clear distinction between the positions of $Ti^{(IV)}$ peaks in NTP and TiO_2 (Fig. 7). The shape and intensity of Ti 2p peak at 458.6 eV, which corresponds to $Ti^{(IV)}$ in TiO_2 remains basically unchanged after 100 GCD cycles supporting the view that titania coating remains practically intact during cycling. The XPS survey spectra of Hf_70 electrodes reveal distinct Hf 4f and 4d peaks at 18 eV and 212–223 eV, respectively. The intensity of these features seems to be only slightly affected by the GCD cycling (Fig. 6c). None of Ti 2p peaks attributable to NTP could be seen in these spectra, although the appearance of F 1s signal after 100 GCD cycles was observed. These results are consistent with the previously discussed observations that hafnia layer stays practically intact during cycling, although some cracks could appear. This could be a reason why F 1 s signal becomes visible in the cycled electrolytes. The results also indicate that 20 nm thick HfO_2 layer is probably insufficiently thick or contiguous to minimize the influence of parasitic processes leading to lower CE and relatively significant NTP capacity fade (Fig. 2). Nevertheless, a 70 nm thick HfO_2 coating seems to effectively suppress the HER and ORR, preventing an increase in local pH and significantly stabilizing the NTP. Therefore, HfO_2 turns out to be the most stable and effective protective ALD coating among the studied materials for aqueous operation of NTP. The only notable disadvantage of hafnia might be its potentially stronger blocking nature in comparison to other oxides, which might be due to its more compact nature leading to slightly lower initial NTP capacities (Fig. 2). However, this limitation could probably be overcome by a careful optimization of the ALD layer thickness.

Self-discharge kinetics.—The self-discharge kinetics of uncoated and 70 nm thick ALD-coated NTP electrodes was studied as well. The electrodes were fully charged at 1C rate and then kept at open-circuit potential (OCP) under ambient conditions. An open beaker-type cell was used in this study and no extra measures were taken to prevent the oxygen access. The results are shown in Fig. 8. In a given setup, it takes about 6 h for the uncoated NTP electrode to fully discharge under open air conditions (Fig. 8 (line 1)). The

alumina coated Al_70 sample shows an extension of self-discharge time to almost 9 h (Fig. 8 (line 2)), which is consistent with higher capacity retention and CE of alumina-coated samples (Fig. 2). In agreement with previous results, the recorded self-discharge time of Hf_70 electrode was the longest among all studied samples and reached ca. 10 h (Fig. 8 (line 4)). This again confirms that 70 nm thick HfO_2 layer was the most effective protective ALD coating studied in this work. Interestingly, the self-discharge of Ti_70 was almost twice as fast as that of Al_70 and even faster than that of uncoated NTP. This comes as another confirmation that previously observed relatively low CE of titania coated NTP electrodes (Fig. 2c) comes from the significant influence of parasitic reactions related to the titania electrochemical activity.

Electrochemical impedance spectroscopy.—The processes taking place at the electrode/electrolyte interface during galvanostatic cycling of uncoated and ALD-coated NTP electrodes were also studied by the electrochemical impedance spectroscopy. The Nyquist plots for the 1st, 2nd, 5th, 10th, 50th and 100th cycle performed at 1C rate in 1 M Na_2SO_4 (aq.) are shown in Fig. 9. In agreement with our previous study,[11] the equivalent circuit used for fitting the measured data consisted of two Randles circuits (inset in Fig. 9c): the low frequency corresponding to charge transfer resistance (R_{CT}) at the electrode/electrolyte interface and the mid-frequency, which is related to the emerging interphasial layer comprising some electrode/coating decomposition products (R_{SEI}). Although the origin of the constant phase element (CPE) is usually ambiguous, it is often observed in real systems. While not strictly necessary for uncoated electrodes, the phase shift effect becomes dominant in the ALD-coated electrodes. It has been shown that varying dielectric coating thickness[38] or energetic heterogeneity[39] can result in such behavior, which would explain why it is more pronounced in the coated samples. The full set of data corresponding to different values of equivalent circuit elements vs cycle number is presented in supplementary data.

In the case of uncoated NTP electrodes, a marked increase in the low frequency semicircle is observed during cycling (Fig. 9a). This could be attributed to the increase in R_{CT} due to degradation of electrode surface and accumulation of various degradation products blocking the ion transfer at the interface (Fig. 10a). The same behavior is observed for the emerging mid-frequency semi-circle and associated R_{SEI} which is attributed to the appearance and growth of an interphasial layer which impedes the motion of Na^+ ions during GCD cycling (Fig. 10a). The EIS data for Al_2O_3-coated samples presented in Figs. 9b and 10b, can be explained by the dissolution of the coating which takes place during the first 10 to 20 cycles as discussed previously. Initially, the coating shows a more pronounced blocking effect with both resistances increasing with cycling as the NTP and alumina start to degrade. However, around the 10th cycle the coating is sufficiently dissolved but there are no insoluble degradation products which would further block the electrode leading to a slight decrease in R_{CT}. However, the remaining part of a coating could still potentially limit the growth of an interphasial layer leading to a stable R_{SEI} (Fig. 10b). The Ti_70 EIS spectra show the most significant increase in R_{CT} during cycling, which becomes especially fast after the 10 initial cycles and reaches the highest values among all studied samples. Considering that titania layer stays intact during 100 GCD cycles, such an increase in R_{CT} could be attributed to the previously discussed electrochemical activity of TiO_2 (see Reaction 1). This activity might not only swell the coating but also lead to locally increasing pH. This tends to accelerate the NTP degradation process leading to very high values of R_{CT} (Fig. 10c). The obtained EIS results for HfO_2 coated NTP are different from the other electrodes. The observed increase in R_{SEI} during cycling is more pronounced than that of R_{CT} (Fig. 10d). One possible explanation for this behavior could be a significantly more compact nature and chemical stability of hafnia coatings. Such coatings provide significant protection of electrode from oxygen access but are also more easily clogged by even a small amount of degradation products. Another explanation, as discussed in the XPS section, could be that some cracks may have appeared in the electrode which in turn would have increased the specific area of the electrode and led to the increase of R_{SEI}. Overall all coatings show higher R_{SEI} values than uncoated electrodes indicating that an ALD coating affected not only the active material - electrolyte interface but also the formation and growth of the aqueous interphasial layer on NTP electrodes.

Conclusions

The atomic layer deposition of conformal layers directly on battery electrodes is an effective and viable strategy to engineer protective coatings for significantly improved electrochemical properties. Three different types of coatings Al_2O_3, TiO_2, and HfO_2 were applied on negative $NaTi_2(PO_4)_3$ electrodes and fully characterized in terms of electrochemical kinetics, charge capacity retention. electrochemical impedance spectra, and surface degradation. The results show that widely used Al_2O_3 does not sufficiently suppress parasitic processes such as oxygen reduction and hydrogen evolution reactions, and is itself dissolved during extended cycling due to increase in local pH. It is very likely that the main protective effect of this coating is more of chemical nature since during dissolution it reacts with hydroxide ions thus temporarily buffering the electrochemical interface. Another widely used TiO_2 coating, on the other hand, is very resistant to increasing pH and remains almost intact during electrochemical cycling. However, we provide another strong evidence that titania itself is electrochemically active in aqueous electrolytes at the typical negative electrode operating potentials. The electrochemical reduction of titania leads to an additional increase in local pH which likely speeds up the NTP degradation leading to even faster capacity decay than in uncoated electrodes. Finally, 70 nm thick HfO_2 is found to be the most (electro) chemically stable and inert ALD coating showing the strongest protective effects for NTP electrodes operating in aqueous electrolytes.

Acknowledgments

This project has received funding from the European Regional Development Fund (Project No. 01.2.2-LMT-K-718-02-0005) under a grant agreement with the Research Council of Lithuania (LMTLT).

ORCID

Laurynas Staišiūnas https://orcid.org/0000-0002-0297-1324
Jurgis Pilipavičius https://orcid.org/0000-0002-0250-1488
Jurga Juodkazytė https://orcid.org/0000-0003-1265-8320
Linas Vilčiauskas https://orcid.org/0000-0002-1256-9777

References

1. J. Kim, Y. Suharto, and T. U. Daim, "Evaluation of electrical energy storage (EES) technologies for renewable energy: A case from the US Pacific Northwest." *Journal of Energy Storage*, **11**, 25 (2017).
2. B. Dunn, H. Kamath, and J.-M. Tarascon, "Electrical energy storage for the grid: a battery of choices." *Science*, **334**, 928 (2011).
3. D. Bin, F. Wang, A. G. Tamirat, L. Suo, Y. Wang, C. Wang, and Y. Xia, "Progress in aqueous rechargeable sodium-ion batteries." *Adv. Energy Mater.*, **8**, 1703008 (2018).
4. Y. Wang, D. Liu, M. Sun, and J. Liu, "Recent progress in electrode materials for aqueous sodium and potassium ion batteries." *Mater. Chem. Front.*, **5**, 7384 (2021).
5. M. Lee et al., "Powder coatings via atomic layer deposition for batteries: a review." *Chem. Mater.*, **34**, 3539 (2022).
6. C. Masquelier and L. Croguennec, "Polyanionic (phosphates, silicates, sulfates) frameworks as electrode materials for rechargeable Li (or Na) batteries." *Chem. Rev.*, **113**, 6552 (2013).
7. C. Delmas, F. Cherkaoui, A. Nadiri, and P. Hagenmuller, "A nasicon-type phase as intercalation electrode: $NaTi_2(PO_4)_3$." *Mater. Res. Bull.*, **22**, 631 (1987).
8. M. Wu, W. Ni, J. Hu, and J. Ma, "NASICON-structured $NaTi_2(PO_4)_3$ for sustainable energy storage." *Nanomicro Lett.*, **11**, 44 (2019).
9. M. Pourbaix, *Atlas of Electrochemical Equilibria in Aqueous Solutions* (Houston, Texas, USA, National Association of Corrosion Engineers) (1974).
10. Z. Li, D. Young, K. Xiang, W. C. Carter, and Y.-M. Chiang, "Towards high power high energy aqueous sodium-ion batteries: The $NaTi_2(PO_4)_3/Na_{0.44}MnO_2$ System." *Adv. Energy Mater.*, **3**, 290 (2013).

11. G. Plečkaitytė, M. Petrulevičienė, L. Staišiūnas, D. Tediashvili, J. Pilipavičius, J. Juodkazytė, and L. Vilčiauskas, "Understanding and mitigation of $NaTi_2(PO_4)_3$ degradation in aqueous Na-ion batteries." *J. Mater. Chem. A Mater. Energy Sustain.*, **9**, 12670 (2021).
12. A. I. Mohamed and J. F. Whitacre, "Capacity Fade of $NaTi_2(PO_4)_3$ in aqueous electrolyte solutions: relating pH Increases to long term stability." *Electrochim. Acta*, **235**, 730 (2017).
13. X. Zhan and M. Shirpour, "Evolution of solid/aqueous interface in aqueous sodium-ion batteries." *Chem. Commun.*, **53**, 204 (2016).
14. A. I. Mohamed, N. J. Sansone, B. Kuei, N. R. Washburn, and J. F. Whitacre, "Using polypyrrole coating to improve cycling stability of $NaTi_2(PO_4)_3$ as an aqueous Na-Ion anode." *J. Electrochem. Soc.*, **162**, A2201 (2015).
15. L. Suo, O. Borodin, T. Gao, M. Olguin, J. Ho, X. Fan, C. Luo, C. Wang, and K. Xu, "Water-in-salt' electrolyte enables high-voltage aqueous lithium-ion chemistries." *Science*, **350**, 938 (2015).
16. W. Wu, S. Shabhag, J. Chang, A. Rutt, and J. F. Whitacre, "Relating electrolyte concentration to performance and stability for $NaTi_2(PO_4)_3/Na_{0.44}MnO_2$ aqueous sodium-ion batteries." *J. Electrochem. Soc.*, **162**, A803 (2015).
17. Y. Shen et al., "High-performance aqueous sodium-ion battery using a hybrid electrolyte with a wide electrochemical stability window." *RSC Adv.*, **10**, 25496 (2020).
18. S. Tutlienė, M. Petrulevičienė, J. Pilipavičius, A. Žarkov, A. Selskis, S. Stanionytė, J. Juodkazytė, and L. Vilčiauskas, "Electrochemical performance of sol-gel synthesized $NaTi_2(PO_4)_3$ - carbon composites as aqueous na-ion battery anodes." *J. Electrochem. Soc.*, **168**, 060545 (2021).
19. B. Zhao, Q. Wang, S. Zhang, and C. Deng, "Self-assembled wafer-like porous $NaTi_2(PO_4)_3$ decorated with hierarchical carbon as a high-rate anode for aqueous rechargeable sodium batteries." *J. Mater. Chem. A Mater. Energy Sustain.*, **3**, 12089 (2015).
20. M. Ritala and J. Niinistö, "Industrial applications of atomic layer deposition." *ECS Trans.*, **25**, 641 (2009).
21. E. Riyanto et al., "A review of atomic layer deposition for high lithium-ion battery performance." *Journal of Materials Research and Technology*, **15**, 5466 (2021).
22. Y. Zhao, K. Zheng, and X. Sun, "Addressing interfacial issues in liquid-based and solid-state batteries by atomic and molecular layer deposition." *Joule.*, **2**, 2583 (2018).
23. F. Yu, L. Du, G. Zhang, F. Su, W. Wang, and S. Sun, "Electrode engineering by atomic layer deposition for sodium-ion batteries: From traditional to advanced batteries." *Adv. Funct. Mater.*, **30**, 1906890 (2020).
24. X. Meng, "Atomic-scale surface modifications and novel electrode designs for high-performance sodium-ion batteries via atomic layer deposition." *J. Mater. Chem. A Mater. Energy Sustain.*, **5**, 10127 (2017).
25. Q. Liu, Z. Hu, C. Zou, H. Jin, S. Wang, and L. Li, "Structural engineering of electrode materials to boost high-performance sodium-ion batteries." *Cell Reports Physical Science*, **2**, 100551 (2021).
26. L. Chen, L. Cao, X. Ji, S. Hou, Q. Li, J. Chen, C. Yang, N. Eidson, and C. Wang, "Enabling safe aqueous lithium ion open batteries by suppressing oxygen reduction reaction." *Nat. Commun.*, **11**, 2638 (2020).
27. A. W. Weimer, "Particle atomic layer deposition." *J. Nanopart. Res.*, **21**, 9 (2019).
28. L. Hu, W. Qi, and Y. Li, "Coating strategies for atomic layer deposition." *Nanotechnology Reviews*, **6**, 527 (2017).
29. Y. S. Jung, A. S. Cavanagh, L. A. Riley, S.-H. Kang, A. C. Dillon, M. D. Groner, S. M. George, and S.-H. Lee, "Ultrathin direct atomic layer deposition on composite electrodes for highly durable and safe Li-ion batteries." *Adv. Mater.*, **22**, 2172 (2010).
30. G. Gečė, J. Pilipavičius, N. Traškina, A. Drabavičius, and L. Vilčiauskas, "Solvothermal engineering of $NaTi_2(PO_4)_3$ nanomorphology for applications in aqueous na-ion batteries." *ACS Sustain. Chem. Eng.*, **11**, 3429 (2023).
31. M. D. Murbach, B. Gerwe, N. Dawson-Elli, and L.-K. Tsui, "*impedance.py*: A Python package for electrochemical impedance analysis." *Journal of Open Source Software*, **5**, 2349 (2020).
32. F. Wang, C.-F. Lin, X. Ji, G. W. Rubloff, and C. Wang, "Suppression of hydrogen evolution at catalytic surfaces in aqueous lithium ion batteries." *J. Mater. Chem. A Mater. Energy Sustain.*, **8**, 14921 (2020).
33. G. Wu, P. Li, C. Zhu, Y. Lei, H. Zhao, T. Li, H. Yue, B. Dou, Y. Gao, and X. Yang, "Amorphous titanium oxide passivated lithium titanium phosphate electrode for high stable aqueous lithium ion batteries with oxygen tolerance." *Electrochim. Acta*, **246**, 720 (2017).
34. N. Makivić, J.-Y. Cho, K. D. Harris, J.-M. Tarascon, B. Limoges, and V. Balland, "Evidence of bulk proton insertion in nanostructured anatase and amorphous TiO_2 electrodes." *Chem. Mater.*, **33**, 3436 (2021).
35. N. Makivić, K. D. Harris, J.-M. Tarascon, B. Limoges, and V. Balland, "Impact of reversible proton insertion on the electrochemistry of electrode materials operating in mild aqueous electrolytes: A case study with TiO_2." *Adv. Energy Mater.*, **13**, 2203122 (2023).
36. W. Liao, J. Yang, H. Zhou, M. Murugananthan, and Y. Zhang, "Electrochemically self-doped TiO_2 nanotube arrays for efficient visible light photoelectrocatalytic degradation of contaminants." *Electrochim. Acta*, **136**, 310 (2014).
37. J. Liu, J. Zhang, S. Cheng, Z. Liu, and B. Han, "DNA-mediated synthesis of microporous single-crystal-like $NaTi_2(PO_4)_3$ nanospheres." *Small.*, **4**, 1976 (2008).
38. C. A. Schiller and W. Strunz, "The evaluation of experimental dielectric data of barrier coatings by means of different models." *Electrochim. Acta*, **46**, 3619 (2001).
39. P. Córdoba-Torres, T. J. Mesquita, and R. P. Nogueira, "Relationship between the origin of constant-phase element behavior in electrochemical impedance spectroscopy and electrode surface structure." *J. Phys. Chem. C*, **119**, 4136 (2015).